A data-driven procedure for the analysis of high strain rate tensile tests via visible and infrared image processing

International Journal of Impact Engineering 199 (2025) 105232

Contents lists available at ScienceDirect

International Journal of Impact Engineering

journal homepage: www.elsevier.com/locate/ijimpeng

A data-driven procedure for the analysis of high strain rate tensile tests via visible and infrared image processing

Marta Beltramo *, Lorenzo Peroni, Martina Scapin

Department of Mechanical and Aerospace Engineering, Politecnico di Torino, Turin, Italy

ARTICLE INFO

Keywords:
Necking
Specimen deformed shape
Plastic flow curve
Strain rate
Self-heating
Database
Strength model identification

ABSTRACT

In the present work, a previously proposed procedure for analyzing quasi-static tensile tests during the post-necking phase is extended to tests at high strain rates. The method utilizes a database built from numerical simulation which correlates the relationship between the equivalent stress and the equivalent plastic strain with the shape of the necking profile and with the engineering stress applied to the specimen. Therefore, such database can be used for characterizing material hardening behavior through appropriate processing of the information collected in the database itself. This significantly reduces the computational effort compared to FE-based inverse methods. More specifically, this paper demonstrates how the proposed method can be used to analyze tensile tests conducted on axisymmetric specimens made of isotropic metallic materials whose plastic behavior depends on both the strain rate and the temperature. Regarding the temperature, the authors focused on the temperature rise caused by material self-heating in dynamic tests, whether under adiabatic conditions or not. From an experimental perspective, both visible and infrared cameras were employed to acquire all the data necessary for analyzing, using the proposed method, the material behavior under dynamic conditions. The proposed approach entailed recording the test with proper spatial and time resolution. The significant advantage is that Digital Image Correlation measurements and evaluation of strains are not necessary, as it is sufficient to extract the external contour of the sample.

1. Introduction

Material response to high-rate loading is of primary importance for the engineering design of metal forming operations, dynamic impact processes, energy absorbers, etc. In these fields, computer modeling of deformation is widely used, but accurate and adequate input of material properties is fundamental to successfully employ this engineering tool. In this sense, one of the crucial properties is the plastic flow stress. In the above-mentioned applications, the material undergoes large deformations while experiencing a broad range of strain rates and temperatures. Thus, it is essential to provide an accurate specification of the flow stress for the range of strains, strain rates, and temperatures imposed on the material. Experimental tests are performed for determining such $\sigma(\varepsilon, \dot{\varepsilon}, T)$ response; in particular, the tension test is widely used. Thanks to adequate techniques, it allows testing from quasi static strain rates up to high strain rates, of about 10^3 s^{-1}. Moreover, it is possible to achieve large strains before fracture.

As is well-known, in tensile tests a displacement is applied to the specimen heads and the sample gradually elongates while reducing its cross-section. Up to a certain point, the load applied to the sample progressively increases and the deformation remains uniform within the gauge length. At a certain point, the deformation localizes in a limited region and the applied load decreases. This localization phenomenon is known to be the main issue in using measurements recorded during the entire test for characterizing material hardening behavior.

Considering only the uniform phase of tests conducted under different loading conditions, analytical formulas can be used to directly determine the hardening behavior. The obtained data can then be fitted with an empirical material model, such as Johnson–Cook [1], or with a physically-based material model, such as Zerilli–Armstrong [2]. A common approach is to divide the calibration process into different steps, each corresponding to the individual calibration of a term of the model (as done in Song and Sanborn [3] for example). However, other fitting strategies could be adopted: Johnson–Cook calibration procedures are thoroughly reviewed by Gambirasio and Rizzi [4].

In some cases, the amount of uniform deformation in ductile metals is limited, as necking occurs soon after yielding. Useful information

* Corresponding author.
E-mail address: marta.beltramo@polito.it (M. Beltramo).

https://doi.org/10.1016/j.ijimpeng.2025.105232
Received 3 October 2024; Received in revised form 1 January 2025; Accepted 25 January 2025
Available online 26 January 2025

about material behavior can still be obtained from post-necking data if it is properly processed to account for the triaxiality and non-uniformity of strain, strain rate, temperature, and stress. It is important to consider that the strain rate during necking can reach values up to 10 times the nominal strain rate [5]. Thus, if the material is sufficiently sensitive to strain rate, this may affect the response even within a single test. Neglecting this aspect may impact the identification results. In the following paragraphs, some strategies that can be adopted to account for strain rate sensitivity within the test are explained. Furthermore, another issue arises, that is how to combine information from different loading conditions to determine the material behavior over a wide range of strain rates and strains.

In the last decades, many researchers have used Digital Image Correlation (DIC) to obtain the kinematic fields ε, $\dot{\varepsilon}$ during the test. In Kim et al. [6] the DIC technique was also used for calculating the acceleration as an alternative to direct load measurement. Various techniques can then be employed to compute the full-field stress starting from kinematic data. These methodologies include the Virtual Field Method (VFM) [7,8]. For example, in the work by Martins et al. [9], the VFM is first used to calibrate a material model representing a single test in order to assess the adequacy of the calibration process and of the chosen constitutive model. Then, the VFM was applied for a calibration process that simultaneously considered different tests. It is also worth mentioning the research by Park et al. [10] where the VFM was exploited for identifying the behavior at different strain rates from the heterogeneous distribution of strain rate during a single dynamic test. However, the DIC technique is subject to some issues, among which the loss of focus on cylindrical specimens and damage to speckle pattern at high temperatures, strain rates and large deformation.

FE-based inverse methods are also commonly used for calibrating material strength models since they accurately consider the actual fields inside the specimen. For these methods, a hardening model is chosen a priori, and parameters are iteratively updated until a good match is achieved between numerical predictions and experimental measurements.

Moreover, FE-based inverse methods could help in purifying the hardening functions from self-heating. Indeed, strain localization in tests at sufficiently high speed may cause a significant temperature rise [11]. Consequently, the identified laws cannot be considered as isothermal and implicitly incorporate thermal softening. In these cases, temperature becomes an additional variable to consider in the plastic flow description. Sometimes, thermal parameters are assumed to be known from tests performed at different temperatures. This may not be rigorously correct since the physics behind the two phenomena is different: high working temperature also affects the structure transformation (grain size, texture, dislocations density, etc.), whereas adiabatic heating mainly affects the dislocations capability to overcome obstacles. Hence, a valid alternative is to consider thermal parameters as optimization variables as well.

Material parameters can be optimized by simultaneously considering different loading conditions. Sometimes the number of optimization variables is reduced by forcing a good fitting of the quasi-static test; so, only temperature and/or strain rate coefficients must be identified with other tests [12–14]. However, the final set of parameters may not be optimal for predicting the material behavior when strain, strain rate and temperature vary simultaneously. A better set of parameters can be obtained by including strain hardening parameters as optimization quantities, in addition to strain rate and temperature coefficients (as done by Milani et al. [15] for compression tests). In this regard, Scapin et al. [16] compared different optimization strategies that differed from each other for the material parameters considered as optimization variables and their range of variation. This analysis focused on compression tests but could also be extended to tension tests.

Nevertheless, previous approaches may not accurately describe each loading condition even if the resulting global behavior could be acceptable. An effective alternative is to optimize each loading condition separately from the others allowing the chosen hardening law to locally approximate material behavior within a certain range of strain rates. In general, the latter approach provides a better description of each test [17], but the problem of uniqueness of the identified model arises. This can be addressed by combining measurements of force and deformed geometry in the optimization process (such as, the necking shape as done in [18,19]). Finally, all the data from the different identified laws could be analytically fitted with a unique strength model. A similar approach was adopted in Yao et al. [20], although it was applied to a damage evolution model for describing the necking phase.

Regardless of the specific optimization strategy adopted, FE-based inverse strategies imply considerable computational effort.

Regarding the objective function of FE-based inverse strategies, in Beltramo et al. [21] it was proved that a strain rate insensitive material model can be identified from a tensile test by using a displacement field as the target (specifically the one associated with the external necking shape of a cylindrical specimen) rather than relying on global quantities like force and displacement. This suggested a unique correlation between the necking profile and the shape of the post-necking plastic flow curve $\sigma_{eq} - \varepsilon_{eq,pl}$. Like all approaches based on numerical optimization, the one proposed in Beltramo et al. [21] was computationally expensive, as many simulations were required to obtain satisfactory results. In particular, information obtained from previous optimizations were not retained, making all these FE-based inverse methods brutal iterative procedures lacking a strategic approach. Hence, in Beltramo et al. [22] the correlation between necking profile and plastic flow curve was exploited: the results of numerical simulations were collected in a database that allowed the correlation of the necking profile with the strain hardening law without the need to recursively simulate different sets of material model parameters.

This idea is further developed in the present paper to be applicable to an experimental campaign of tensile tests performed at different speeds on axisymmetric samples, under the assumption of isotropic Von Mises plasticity. It is worth underlining again that no numerical optimization based on FE simulations was used. Conversely, the method consists of searching for the best profile within a database, which contains a series of 1250 different sets of parameters capable of describing the plastic flow curve $\sigma_{eq} - \varepsilon_{eq,pl}$ of a metallic material. By applying proper techniques and considerations (which will be detailed in Section 2), the material behavior at a given time can be approximated using the database material model that gives the closest necking profile. This approach allows for the estimation of not only the strain and strain rate distribution on the specimen's outer surface but also the equivalent stress distribution. Regarding the temperature, since it depends not only on the current state, but also on the material's past history, it is measured using an infrared camera.

This approach is less computationally expensive than FE-based inverse techniques. Moreover, from the experimental point of view, only the external contour of the sample, rather than DIC measurements, is required for evaluating the deformation.

In Section 2 the proposed methodology is explained in detail, and an experimental case study shows how the approach can account for strain rate effects within a single test. Then, the proposed method of analysis is applied to experimental tensile tests performed on martensitic stainless steel (17-4 PH H900) at different test speeds. This shows how the proposed method can be used in an experimental campaign for characterizing a material over a wide range of strains and strain rates, dealing also with self-heating, whether under adiabatic conditions or not. In Section 3 the experimental setup is presented and in Section 4 data are analyzed with the proposed method and critically discussed.

2. Proposed methodology

The proposed strategy consists of gaining information about material behavior starting from axisymmetric necking profile and utilizing a

database built from FE simulations of tensile tests. In Beltramo et al. [22] this method was applied to identify the material response during tensile tests on materials and conditions in which the effects of strain rate were negligible. In Scapin and Beltramo [23] it was shown a preliminary application to materials that are sufficiently sensitive to strain rate that even the response within a single test is influenced by the strain rate variations occurring during necking. Significative advancements in this latter aspect will be presented in the present paper.

The key idea is that, although the response of the material during a single test is affected by strain rate variation and heterogeneity, a strain rate insensitive database can still be used to infer some physical quantities that cannot be experimentally measured. In other words, a strain rate sensitive material could be approximated at each instant by a different strain rate insensitive law. Section 2.1 presents some background on the database approach and explains how a strain rate insensitive database can be used to analyze strain rate sensitive materials. Section 2.2 offers details about the establishment of the database. Section 2.3 describes the proposed procedure, and finally, Section 2.4 presents the experimental application to an isothermal test where strain rate effects are appreciable.

Before moving on to these subsections, a general overview of the method is provided in Fig. 1, which schematically represents the procedure.

The strategy entails conducting a monotonic tensile test during which the load history is monitored and both visible and infrared images are acquired. At each time instant t_i, the necking profile is used to identify the model from the database that best describes the material at that moment. This model, then, provides a reasonable approximation of the strain, strain rate, and stress experienced by material points on the specimen's surface at that time (with the load and the speed at that instant appropriately considered, as detailed in Section 2.3). These quantities are denoted as $\varepsilon_{eq,pl}(x,t_i)$, $\dot{\varepsilon}_{eq,pl}(x,t_i)$, $\sigma_{eq}(x,t_i)$ in Fig. 1. Since these represent the spatial distributions of strain, strain rate, and stress along the axial direction at a fixed time, they will henceforth be referred to as $\varepsilon_{eq,pl}(x)$, $\dot{\varepsilon}_{eq,pl}(x)$, $\sigma_{eq}(x)$.

A key advancement of the proposed method is the ability to estimate the strain rate at different points on the specimen's outer surface during the post-necking phase of tensile tests, without the need for speckle painting or extremely high-frame-rate imaging. As previously mentioned, if the material behavior is well described by a specific material model from the database at a given time, this model provides a reasonable estimate of the strain rate distribution at that moment (as shown in Section 2.4), provided that a monotonic tensile test is analyzed. This is possible because the strain rate is a differential quantity that depends only on how strain evolves in an infinitesimally small neighborhood of the time considered.

Drucker's postulate for isotropic Von Mises plasticity implies a unique relation between plastic strain rates and stresses. Therefore, the stress at various points on the specimen's outer surface can be estimated using the model from the database and the load measured at that time (to ensure the same resulting force).

By applying the proposed method to a single necking profile, a locus of points in the $\varepsilon_{eq,pl} - \dot{\varepsilon}_{eq,pl} - \sigma_{eq}$ space is obtained, representing the specimen's condition at that time. It is important to emphasize that, although the considered configuration may result from different strain rate and temperature sensitivities, the strain, strain rate, and stress distributions on the specimen's outer surface are unambiguously determined from the external profile at that time during the post-necking phase of tensile tests (properly accounting for the

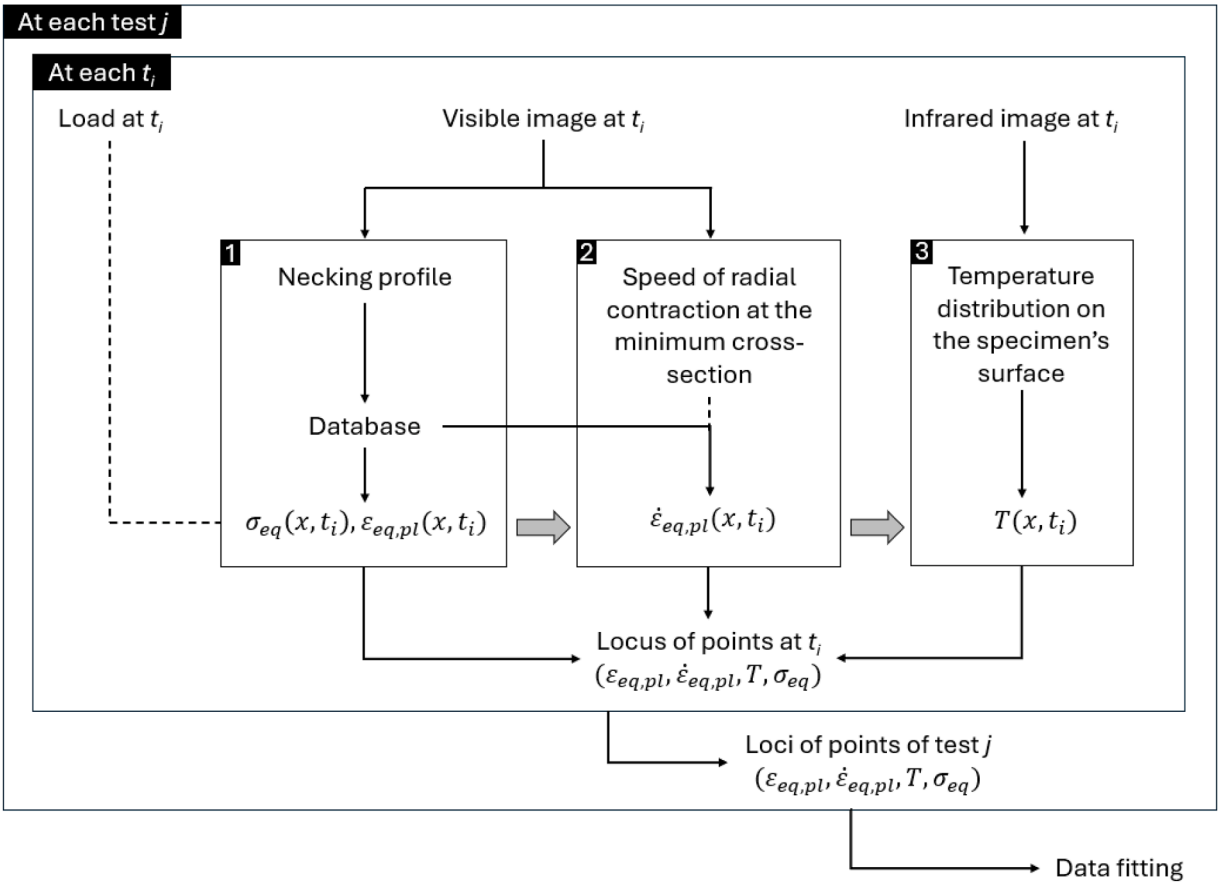

Fig. 1. Schematic representation of the procedure; dashed lines indicate information used for correcting the distributions obtained from the database (according to Section 2.3).

instantaneous test speed and load).

Regarding temperature, different considerations are required, as it depends on the stress-strain history. To compute the temperature distribution at the considered time, it would be essential to track the stress and strain history of material points until the considered configuration. Furthermore, some a priori assumptions regarding the conversion of plastic work into heat would be necessary. Therefore, in the proposed method, the temperature distribution at each time is not computed but, instead, measured experimentally.

To summarize, the proposed approach identifies, for each time instant, a locus of points in the $\varepsilon_{eq,pl} - \dot{\varepsilon}_{eq,pl} - T - \sigma_{eq}$ space, representing the specimen's condition at that time. This procedure can, then, be applied to different time points within the same test to capture the material response during the post-necking phase (of that test). Additionally, the method can be applied to different monotonic tensile tests, allowing for exploration of a broader domain. The final output is a 4D point cloud, to which data fitting techniques can be applied to derive a material model for FE simulations.

2.1. Database approach background

As already mentioned, the proposed strategy is based on the principle that the necking shape, in a tensile monotonic test on round specimens, intrinsically contains information about the strain, strain rate, and stress distributions on the specimen surface along the axial direction at the considered time. Since it is not straightforward to analytically derive an expression relating the necking shape to equivalent plastic strain, strain rate, and stress, the authors decided to rely on a database built from FE simulations.

To better understand the database approach, consider that, in a generic necking configuration, different material points on the specimen surface experience different strain, strain rate and temperature values, leading to different values of equivalent stress (as shown in Fig. 2). Generally, due to the nature of the phenomenon, material points farther from the neck tend to have lower values of strain, strain rate and temperature than that at the center, where maximum values are reached. Moreover, since elastic unloading could occur during necking, a portion of the material points lies in the elastic regime (up to ε^* in Fig. 2).

If the material is strain rate insensitive and temperature remains constant during the test (isothermal test), it was proved in Scapin and Beltramo [23] that, beyond the point of instability, a unique correlation exists between the curve $\sigma_{eq} - \varepsilon_{eq,pl}$ followed by material points on the specimen surface and all the shapes assumed by the sample during the test. In other words, the different necking shapes observed at various instants during the test are all correlated with the same curve $\sigma_{eq} - \varepsilon_{eq,pl}$. Indeed, for strain rate insensitive materials, all material points follow the same path that coincides with the hardening law $\sigma_{eq} - \varepsilon_{eq,pl}$. This is why in Beltramo et al. [21,22], it was possible to use a single highly deformed necking configuration to identify the post-necking strain hardening law. Conversely, when strain rate sensitivity is such that its effect can be observed even within a single test, special care is required in applying the previous approach, because it cannot be assumed that all material points follow the same path.

The paths followed by material points for low and high strain rate sensitivity can be illustrated through FE simulations. This is depicted in Fig. 3, where different superficial material points are denoted with capital letters from A to E. In case of strain rate independent materials (Fig. 3a), all the paths overlap until elastic unloading occurs. Conversely, for strain rate dependent materials (Fig. 3b), the paths progressively deviate from that of the profile center A, because they experience different strain rates during deformation.

If the material is sensitive to strain rate, a correlation between the curve $\sigma_{eq} - \varepsilon_{eq,pl}$ and the specimen shape still exists: a single necking shape correlates the equivalent strain of the superficial material points with the corresponding equivalent stress generated at that time by the applied load (engineering stress) and the triaxiality induced by the specimen shape itself. However, while in strain rate insensitive materials different necking shapes are all correlated with the same $\sigma_{eq} - \varepsilon_{eq,pl}$ curve, in strain rate sensitive materials each necking shape is correlated with a different curve. In strain rate sensitive materials this locus of points, corresponding to the equivalent stress values of the superficial material points, does not represent, as in [22,23], the plastic flow curve of all material points. Instead, it represents the configuration that superficial material points assume on the surface $\sigma_{eq}\left(\varepsilon_{eq,pl}, \dot{\varepsilon}_{eq,pl}, T\right)$ at that instant. Typically, strain and strain rate cause this locus to be an increasing curve in the plane $\sigma_{eq} - \varepsilon_{eq,pl}$. However, a decreasing curve may occur in case of significant softening caused by self-heating. Indeed, the procedure remains valid even when the sample heats up due to plastic deformation during the test and even if it does not occur in completely adiabatic conditions.

To summarize, the most important outcome is that a single necking shape of a tensile test can give information about the stress configuration of the material points on the specimen surface. However, in strain rate sensitive materials, since different material points follow different paths, it is crucial to consider multiple shapes to obtain a set of assumed stress configurations that reflects the visco-thermo-plastic behavior of the material. Each necking shape provides information about the range of equivalent strains and strain rates experienced at that instant by superficial material points, provided that $\dot{\varepsilon}_{eq,pl} > 0$. This last condition determines the range of equivalent plastic strain $\left[\varepsilon^{\min}_{eq,pl}, \varepsilon^{\max}_{eq,pl}\right]$ associated with a particular shape. As deformation proceeds, subsequent shapes provide analogous information over a range of strain which gradually shifts to higher values. This is because of the nature of the phenomenon: $\varepsilon^{\max}_{eq,pl}$ increases due to continuous localization; $\varepsilon^{\min}_{eq,pl}$ increases due to progressive unloading. Therefore, analyzing different necking configurations enables the exploration of a broader strain domain, which is essential for strain rate sensitive materials.

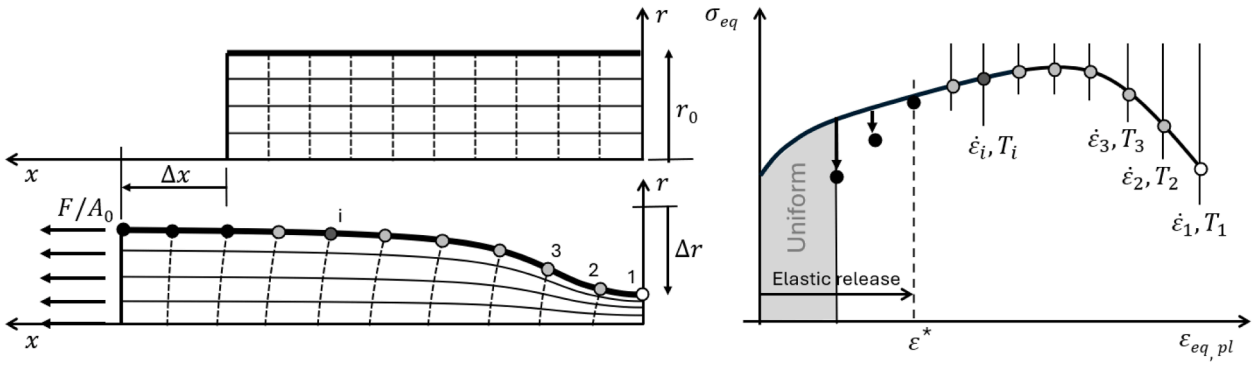

Fig. 2. Correlation between necking shape and hardening law in strain rate insensitive models.

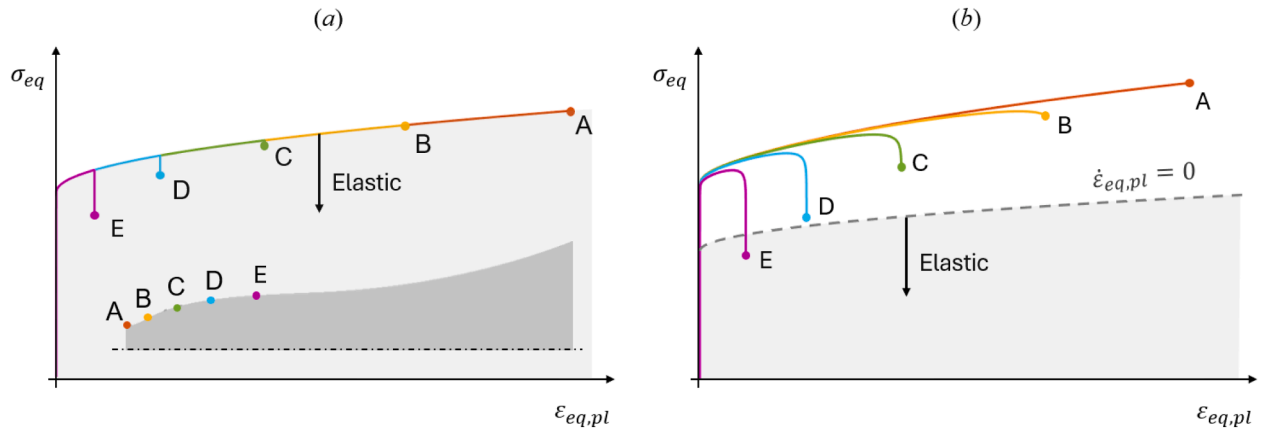

Fig. 3. Deformation paths followed during a tensile test by different material points (A, B, C, D, E) on the specimen surface for strain rate insensitive materials (*a*) and strain rate sensitive materials (*b*).

Additionally, different loading conditions can be examined, facilitating the acquisition of a comprehensive set of stress configurations related to the material visco-thermo-plastic behavior. The obtained results can then be fitted with an appropriate mathematical model.

2.2. Numerical database

From a practical standpoint, the proposed approach utilizes a strain rate insensitive database to establish the relationship between necking profiles $r(x)$ and superficial distributions along the axial direction of equivalent plastic strain $\varepsilon_{eq,pl}(x)$, equivalent plastic strain rate $\dot{\varepsilon}_{eq,pl}(x)$ and equivalent stress $\sigma_{eq}(x)$.

The database was created by simulating monotonic tensile tests on isotropic materials with Von Mises yield criterion and various strain hardening behaviors. The simulations were conducted with the commercial FE code Ansys LS-DYNA. As schematically depicted in Fig. 4, the database collects the results in terms of force, radial speed at the minimum cross-section and a series of necking shapes together with the corresponding superficial distributions of strain, strain rate, and stress (i.e., distributions along the axial direction obtained from elements on the outer surface).

The main features of the model are summarized hereinafter, while a detailed description can be found in Beltramo et al. [22].

Axisymmetric shell elements with one integration point were used to model cylindrical specimens. Only half of the specimen was modeled by imposing the symmetry at one end. Since the explicit solver was used, the authors ensured that the motion applied to the other end did not generate inertial effects. The choice of a cylindrical specimen was made to ensure the applicability of the method to samples with different aspect ratios, as demonstrated in Beltramo et al. [22]. Regarding the mesh, element distortion at large deformations was minimized by adopting an initial aspect ratio that led to regular element shapes during necking development (see Fig. 4). Nevertheless, simulation results were saved into the database only until element distortion was limited.

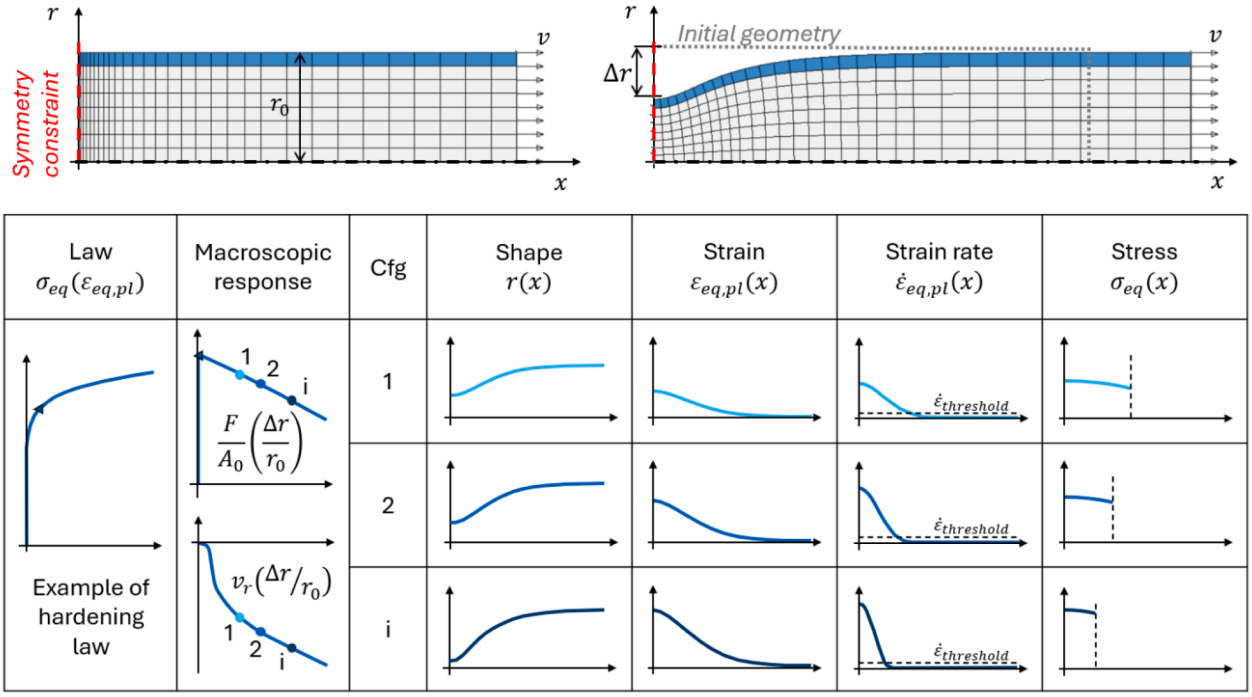

Fig. 4. On the top: FE model of the cylindrical specimen at the initial and at a necking deformed configuration (the elements considered for strain, strain rate and stress distributions are colored in blue). On the bottom: schematic representation of the data saved in the database for each FE simulation ("cfg" stands for "configuration").

Regarding the elastic behavior, elastic deformation occurs during both loading and the progressive unloading that takes place during necking. However, elastic deformations are reasonably negligible compared to the plastic deformations reached in the post-necking phase, so the elastic properties are fixed at predefined values in FE models used to build the database.

The simulations varied only in their strain hardening law. Since self-heating is a key focus of this paper, the database includes not only linear, power-law and saturating laws, but also non-monotonic curves to account for thermal softening.

It is worth reminding from Beltramo et al. [22] that hardening laws differing only in the pre-necking phase and in the scale of stress values are analogous in terms of necking profile and engineering curve. Therefore, only one hardening law from this extensive set needs to be simulated, since all the others would provide redundant data. These analogies allow for a reduction in the size of the database. Consequently, the information extracted from the database must be properly adjusted when applying the method, as detailed in the following section. In this work, an additional strategy to reduce the database size was to avoid simulating all possible strain rate dependencies, instead a strain rate insensitive database was used to analyze strain rate sensitive materials.

2.3. Procedure

The following paragraphs explain how the proposed method works.

Starting from the images acquired during the experimental tensile test, the evolution of the necking external contour is determined. By exploiting material isotropy and the axisymmetric sample geometry, an average semi-profile is considered for each frame. The experimental semi-profiles are then analyzed one by one according to the procedure described below.

An algorithm implemented in MATLAB searches for the closest necking shape in the database. Specifically, the comparison between the experimental profile and the database is done in terms of relative shape rather than absolute size, as explained in Beltramo et al. [22]. The output of this search consist of a database profile $r_{DB}(x)$ and a geometry scaling coefficient k_g: the pairs (x_{DB}, r_{DB}), if properly scaled to $(x_{DB}/k_g, r_{DB}/k_g)$, are overlapped with the experimental profile $r(x)$ (see Fig. 5a).

The shape from the database that best fits the experimental one is associated with specific superficial distributions $\varepsilon_{eq,plDB}(x)$, $\dot{\varepsilon}_{eq,plDB}(x)$, $\sigma_{eqDB}(x)$ through the database itself. Starting from this information, the corresponding experimental distributions $\varepsilon_{eq,pl}(x)$, $\dot{\varepsilon}_{eq,pl}(x)$, $\sigma_{eq}(x)$ can be determined through appropriate operations. This is because, as mentioned earlier, analogous hardening laws exist (this is the analogy already exploited to reduce the size of the database).

Since the numerical and the experimental profile have the same relative shape, the distribution of post-necking equivalent plastic strain is the same. Hence, the database first enables the determination of post-necking equivalent plastic strain, to which the equivalent plastic strain at the necking onset can simply be added. In some cases, estimating the maximum uniform deformation to be added can be challenging, but it can be derived from the coefficient k_g. It results that the pairs $(x_{DB}, \varepsilon_{eq,plDB})$, when properly modified to $(x_{DB}/k_g, \varepsilon_{eq,plDB} + 2\ln(k_g))$, give an estimate of the experimental $\varepsilon_{eq,pl}(x)$ (see Fig. 5b).

Regarding the equivalent plastic strain rate, the database allows to estimate the actual distribution by knowing the instantaneous test speed v and the coefficient k_g. With a diameter-based approach, v represents the radial speed of the central point (instead of the axial speed). The radial speed can be estimated from the history $r(t)$ at the minimum cross-section. This approach eliminates the need for axial measurement when applying the proposed method, making it suitable for tests with back-light illumination. The experimental $\dot{\varepsilon}_{eq,pl}(x)$ can be estimated by adjusting the pairs $(x_{DB}, \dot{\varepsilon}_{eq,plDB})$ to $(x_{DB}/k_g, \dot{\varepsilon}_{eq,plDB} k_g v/v_{DB})$, as shown in Fig. 5c. This is one of the reasons the proposed approach is promising: it allows for the estimation of the strain rate distribution, a quantity that is often difficult to determine experimentally (also because such quantities defined as derivatives are usually very noisy). Other methods, such as FE-based inverse techniques, can give this estimate only after the material has been characterized, making it a posteriori evaluation.

Finally, regarding the equivalent stress, the procedure compares the

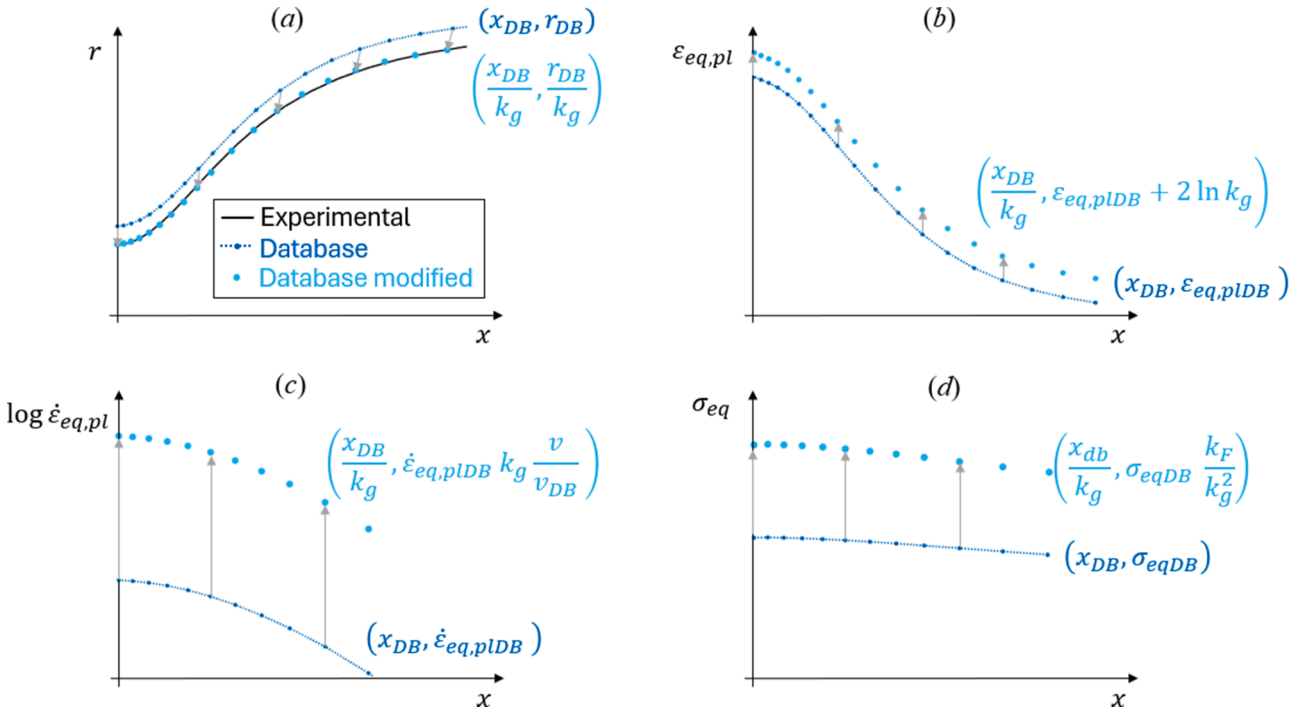

Fig. 5. Schematic representation of the procedure to be applied to each necking configuration. (*a*) shows the semi-profile of the database that, optimally scaled, overlaps the experimental one. (*b*), (*c*) and (*d*) show the operations to be performed on the strain, strain rate and stress distributions of the database in order to estimate the experimental ones.

engineering radial curves $\frac{F}{A_0} - \frac{\Delta r}{r_0}$ of the database and of the experiment (being Δr the radial contraction at the minimum cross-section), as explained in Beltramo et al. [22]. This allows to determine the coefficient k_F that properly modifies the pairs (x_{DB}, σ_{eqDB}) into $\left(x_{DB}/k_g, \sigma_{eqDB}k_F/k_g^2\right)$, leading to an estimate of $\sigma_{eq}(x)$ (see Fig. 5d). It is worth underlining that an advantage of the proposed method, even more beneficial than the ability to estimate the superficial distribution of strain rate (which could also be done through DIC, even if with more experimental effort), is the ability to determine the superficial distribution of equivalent stress.

To conclude, the identified distributions represent a locus of points in the space $\varepsilon_{eq,pl} - \dot{\varepsilon}_{eq,pl} - \sigma_{eq}$ where only the points with $\dot{\varepsilon}_{eq,pl} > 0$ should be considered to extract information about the plastic flow curve.

This procedure must then be repeated for different necking configurations to obtain a point cloud and to ensure the consistency of the results while exploring a broader domain.

The entire procedure can be applied to tests under various loading conditions, and in the case of dynamic tests it can also be combined with temperatures directly measured on the sample (for example, using an infrared camera). Hence, the complete material response $(\varepsilon_{eq,pl}, \dot{\varepsilon}_{eq,pl}, \sigma_{eq}, T)$ can be estimated.

While many researchers do not measure temperature directly and instead account for it through numerical simulations using a Taylor–Quinney coefficient, this work aims for a direct measurement of temperature without relying on any simulations.

It is known that under adiabatic conditions, temperature could be estimated with the following equation:

$$T = T_r + \frac{\beta}{\rho c_p}\int_0^{\varepsilon} \sigma_{eq} d\varepsilon_{eq,pl}, \tag{1}$$

by using the room temperature T_r, and assuming the Taylor–Quinney coefficient β, the density ρ, and the specific heat c_p. However, computing the plastic work required by Eq. (1) is immediate only for strain rate insensitive materials because all material points follow the same path (that the proposed approach identifies). Instead, in strain rate sensitive materials, it would be necessary to follow the evolution of a material point from a certain configuration to the next, which is not straightforward. Hence, the authors chose to acquire the temperature experimentally.

2.4. Experimental application to a strain rate sensitive material

Before moving on to test the methodology against experimental situations in which both strain rate and temperature influence the material response, it is worth analyzing an experimental case influenced solely by strain rate. In this section, the method is applied to existing experimental data from a quasi-static tensile test on pure molybdenum [23]. This material is highly sensitive to strain rate [19,24], allowing for the examination of an isothermal test in which the response is affected by heterogeneity and variation of strain rate, without any influence from temperature.

A series of experimental necking shapes were considered and some of the corresponding semi-profiles are shown in Fig. 6a, and compared with the best shapes found in the database. Using the database, it was possible to associate each configuration with a curve $\sigma_{eq}(\varepsilon_{eq,pl})$, defined over the range of strains achieved on the specimen surface for that configuration. The curves $\sigma_{eq}(\varepsilon_{eq,pl})$ of the database found for the necking shapes reported in Fig. 6a are shown in Fig. 6b, together with the true curve and the average curve which can be regarded as a first approximation of the hardening law.

If a FE simulation of the tensile test under analysis was performed by using the average curve as the hardening law of a strain rate insensitive material, the results would accurately predict the experimental force (see Fig. 6c), but would not match the experimental deformed profiles (as shown in Fig. 6a). This discrepancy arises because strain rate sensitivity was neglected, even though it is known to affect the material response. Indeed, the database curves of Fig. 6b were found to not be overlapped because strain is not the only variable governing the plastic

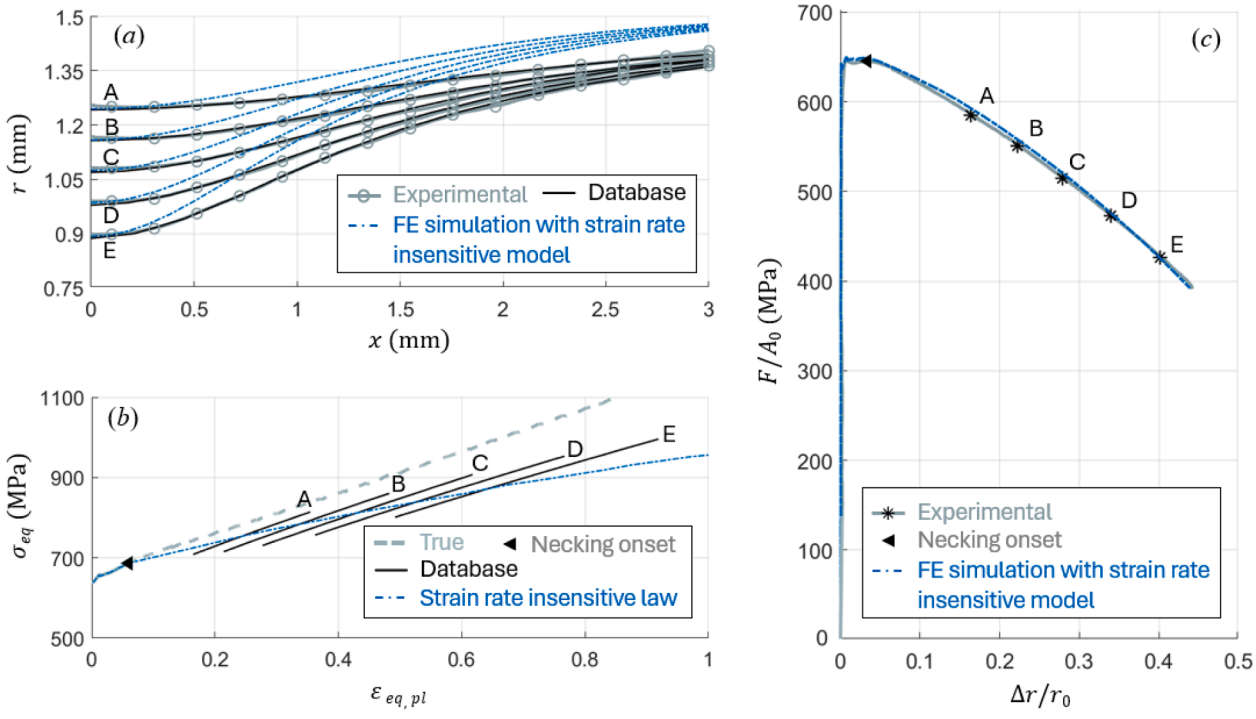

Fig. 6. Application of the proposed method to an isothermal test on pure molybdenum and comparison with a FE simulation having as input a strain rate insensitive hardening law.

deformation: strain rate also plays an essential role. Thus, as explained in Section 2.1, the black lines of Fig. 6b do not represent the plastic flow curve but loci of points describing the stress configuration of superficial material points at different instants.

As presented in Section 2.3, the database can be used for estimating the strain rate distribution (see Fig. 7b) and, consequently, to find loci of points in the space $\varepsilon_{eq,pl} - \dot{\varepsilon}_{eq,pl} - \sigma_{eq}$. The resulting point cloud was fitted with a function $f(\varepsilon_{eq,pl}, \dot{\varepsilon}_{eq,pl})$, that was subsequently used as the material hardening law in FE simulation of the test.

The results are reported in Fig. 7, demonstrating that the prediction for both force and deformation is accurate (see Fig. 7a and c respectively). This indicates that the identified law effectively describes the material behavior under that loading condition. Hence, the similarity shown in Fig. 7b between the strain rate distributions obtained from the FE simulation and those estimated from the database suggests the ability of the method to provide a reliable estimate of this quantity. This finding is crucial, as otherwise the experimental measurement of the strain rate, being defined as derivative, would be very noisy.

More generally, the experimental case study presented in this section highlights that the proposed method can adequately account for the strain rate effect during a single test on a material highly sensitive to strain rate. Consequently, in the next sections the proposed method will be applied to an experimental campaign for investigating the combined effect of strain rate and temperature in dynamic tests.

3. Experimental setup

The proposed methodology was applied in a test campaign varying the strain rate of the tensile tests. The material under investigation was martensitic stainless steel 17-4PH (H900), which is moderately sensitive to strain rate and tends to exhibit significant self-heating due to its low thermal conductivity.

Experimental tensile tests were conducted at room temperature at different test speeds: nominally 0.01, 1, 10, 10^3 s^{-1}. Intermediate test speeds were selected on the basis of the behavior exhibited by the materials in the dynamic tests. Although five tests were conducted for each loading condition, only one test per condition is presented for clarity, due to the low dispersion of the results. The test selected for each condition was the one closest to the average of all tests conducted under that same loading condition.

Low and intermediate strain rate tests were conducted using a Dartec-HA100 servo-hydraulic testing machine. The higher strain rate condition (nominally 10^3 s^{-1}) was achieved with a Split Hopkinson tension setup in direct configuration (for a detailed description, see Scapin et al. [19]).

The proposed approach required recording the test with adequate spatial and temporal resolution. Backlight illumination was used to ensure a high signal-to-noise ratio and careful attention was given to achieve proper exposure. Additionally, thermal effects can arise when the test speed is such that the specimen cannot fully dissipate energy into the surrounding environment, causing some energy to remain within the material and leading to a rise in temperature. Depending on the material, this temperature increase can be significant, resulting in observable thermal softening. To monitor temperature changes, the tests were also recorded using an infrared high-speed camera (FLIRX6900sc SLS).

Table 1 and Fig. 8 summarize the details of all experimental tests.

Cylindrical dog-bone specimens with a gauge length of 5 mm and a gauge diameter of 3 mm were used, following the geometry adopted by the authors in previous works [19]. While this geometry is not standard for quasi-static tests, it was chosen to guarantee consistency, with specimens designed for Hopkinson bar tests, across all loading conditions.

For the quasi-static tests, a high-resolution camera equipped with telecentric optics and illumination was used. This equipment minimized distortion and perspective errors, as explained in detail in Scapin and Beltramo [23]. For the intermediate tests, a high-resolution high-speed camera was employed, and infrared images were captured synchronously with visible images. In the high strain rates test, two high-resolution high-speed cameras were used: Photron FASTCAM SA5 operating at 50,000 fps with a resolution of 640 × 208 to analyze necking shape evolution and Photron FASTCAM Nova S6 operating at 100,000 fps with a resolution of 256 × 128 for more accurate and

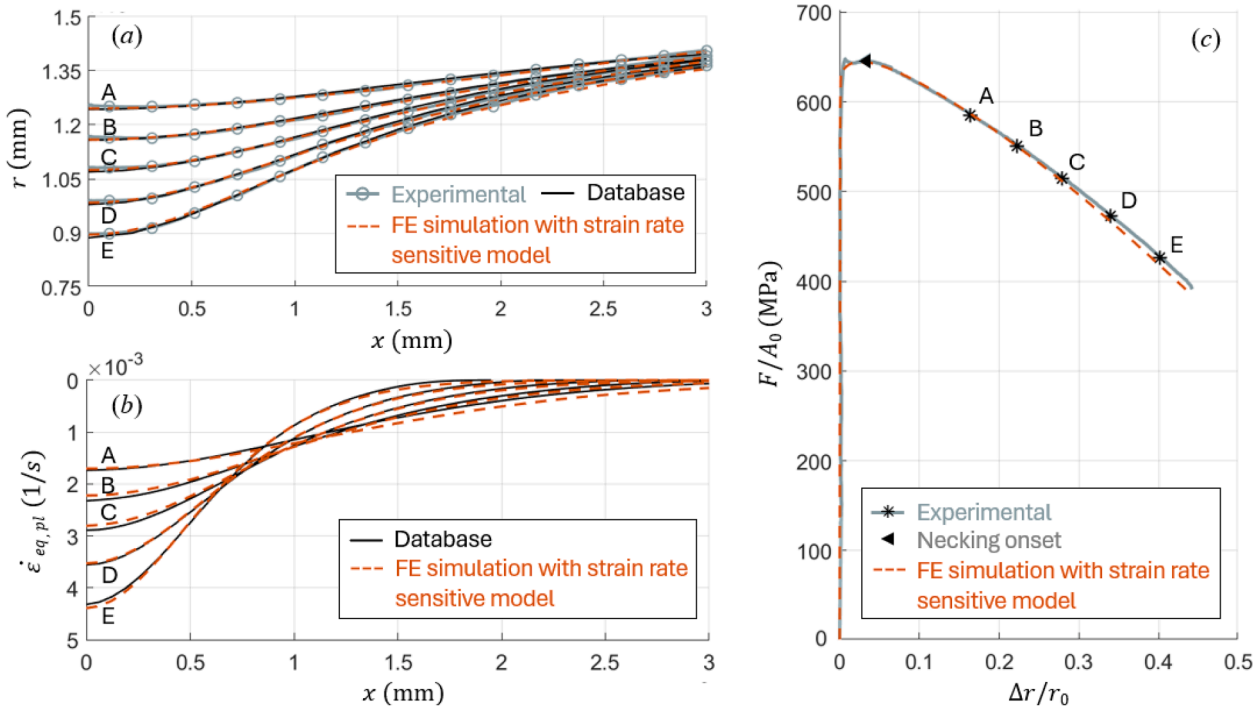

Fig. 7. Application of the proposed method to an isothermal test on pure molybdenum and comparison with a FE simulation having as input a strain rate sensitive hardening law.

Table 1
Details of experimental tests.

Test type	Nominal strain rate (1/s)	Equipment	Camera	Resolution (px × px)	Frame rate (fps)	FLIRX6900sc SLS Resolution (px × px)	FLIRX6900sc SLS Frame rate (fps)
1	0.01	Dartec HA100	Opto Engineering ITA81-GM-20C	2856 × 2848 11 µm/px	1	–	–
2	1	Dartec HA100	Photron Mini AX50	1024 × 1024 24 µm/px	500	640 × 512 45 µm/px	500
3	10	Dartec HA100	Photron Mini AX50	1024 × 1024 24 µm/px	5,000	640 × 88 45 µm/px	5,000
4	1,000	SHTB	Photron SA 5	640 × 208 37 µm/px	50,000	640 × 16 45 µm/px	16,040
			Photron Nova S6	256 × 128 15 µm/px	100,000		

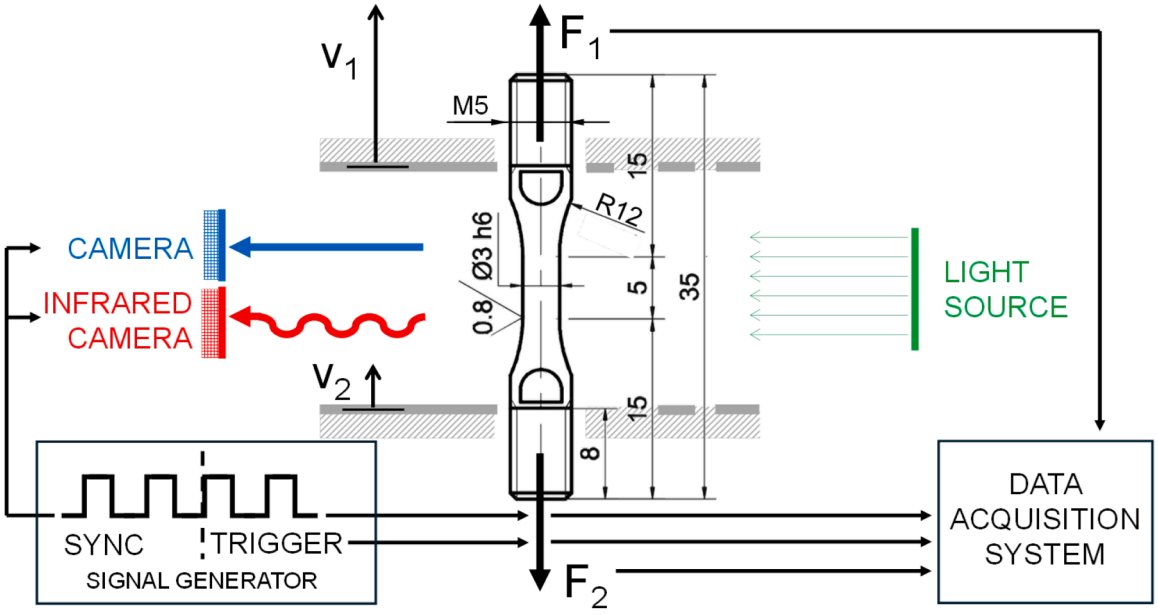

Fig. 8. Schematic representation of the experimental tests and acquired data.

frequent measurements of the minimum radius. Thermal images were acquired at 16,040 fps and with a resolution of 640 × 16.

Fig. 9 presents some visible images acquired during the SHTB test, showing heat release (with surface temperatures exceeding 350 °C) and cup-and-cone fracture. This type of fracture is known to result from the formation of microcracks within the specimen [25]. To minimize the influence of void nucleation and coalescence, the authors concentrated their analysis on the phase of the test that was sufficiently distant from significant reductions in mechanical strength.

All visible images were post-processed in MATLAB to extract the

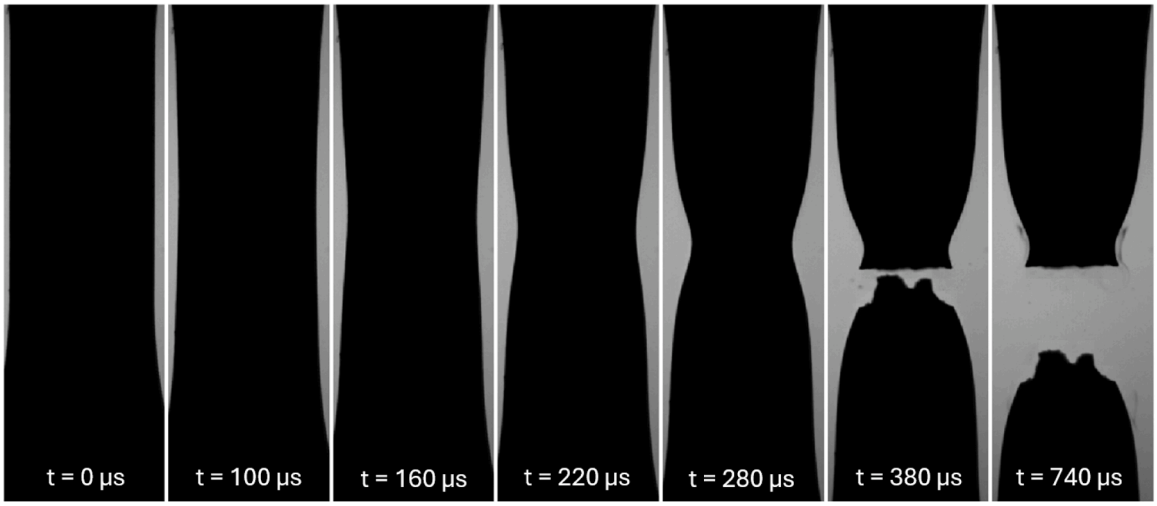

Fig. 9. Some recorded images from a test on the SHTB.

external contour of the specimen. Specifically, an image segmentation technique based on k-means clustering was used, followed by edge detection to identify specimen's silhouette.

Infrared images were also post-processed, to obtain the temperature distribution along the axial direction. Fig. 10 illustrates the analysis of a typical infrared image acquired during the tests.

Assuming axialsymmetry, the superficial temperature measured by the infrared camera is not expected to vary at each fixed axial coordinate. Therefore, each series of pixels aligned with the axial direction theoretically provides redundant information. By reading the image column by column (see Fig. 10a), multiple temperature distributions could be obtained and then averaged to produce a single temperature distribution. Actually, only some columns were considered, to avoid errors due to light reflection or boundary effect. Referring to Fig. 10a, only the columns in region A and B were considered, and the corresponding temperature distributions are plotted with dots in Fig. 10b. Exploiting the assumption of axialsymmetry again, the top and bottom portions of the distribution (identified by the position of maximum temperature) were also averaged. The resulting temperature semi-profiles will be compared in Fig. 14 with those predicted by the identified material model.

As shown in Fig. 10, data scatter was higher in regions with lower temperatures, farther from the necking center. However, as detailed in Section 4, these regions of the specimen were also the ones that were no longer in the plastic domain. Hence, being outside the region of interest, these parts were automatically excluded from the subsequent analysis.

4. Data analysis and discussion

For all the tests, uniform deformation was analyzed using a diameter-based approach. This choice was made because the tests were recorded with backlight illumination, which prevented the tracking of surface markers needed for the traditional length-based approach. Based on the assumptions of uniaxial stress and volume conservation (while reasonably neglecting elastic deformation), some studies [26,27] expressed σ_{eq} and ε_{eq} in terms of radial measurements using the following relationships for the pre-necking phase:

$$\sigma_{eq} = \sigma_a = \frac{F}{\pi r^2}, \tag{2}$$

$$\varepsilon_{eq} = \varepsilon_a = -2\varepsilon_r = -2\varepsilon_h = 2\ln\frac{r_0}{r}, \tag{3}$$

being r_0 the initial gauge radius and r the current radius. The subscripts a, r, h refer to the axial, radial, and hoop component respectively. These equations allow estimating σ_{eq} and ε_{eq} during uniform deformation starting from radial rather than axial measurements.

Attention should also be paid to the evaluation of strain rate. Generally, tests are not performed at a constant strain rate: as uniform deformation proceeds, the strain rate varies due to the increasing length of the specimen. Theoretically each point $(\varepsilon_{eq}, \sigma_{eq})$ should be associated with the correct $\dot{\varepsilon}_{eq}$ even during uniform deformation [28]. To compute the strain rate, the following equation applies in a length-based approach for the pre-necking phase:

$$\dot{\varepsilon}_{eq} = \frac{1}{L}\frac{dL}{dt} = \frac{v(t)}{L}. \tag{4}$$

Similar to equivalent strain, the equivalent strain rate can be expressed in terms of radial measurements:

$$\dot{\varepsilon}_{eq} = -\frac{2}{r}\frac{dr}{dt}. \tag{5}$$

Considering the variation of $\dot{\varepsilon}_{eq}$ during the pre-necking phase of a single test may be crucial for tests with high effect of strain rate [29]. However, in the experimental campaign of this research, necking occurred soon after yielding, resulting in a negligible strain rate variation during uniform deformation. This observation, together with the known logarithmic effect of strain rate in the thermally activated region, supports the conclusion that strain rate effects can be considered negligible within a test, during pre-necking.

In dynamic tests, temperature is also of interest; however, no temperature rise during uniform deformation was observed in any of the

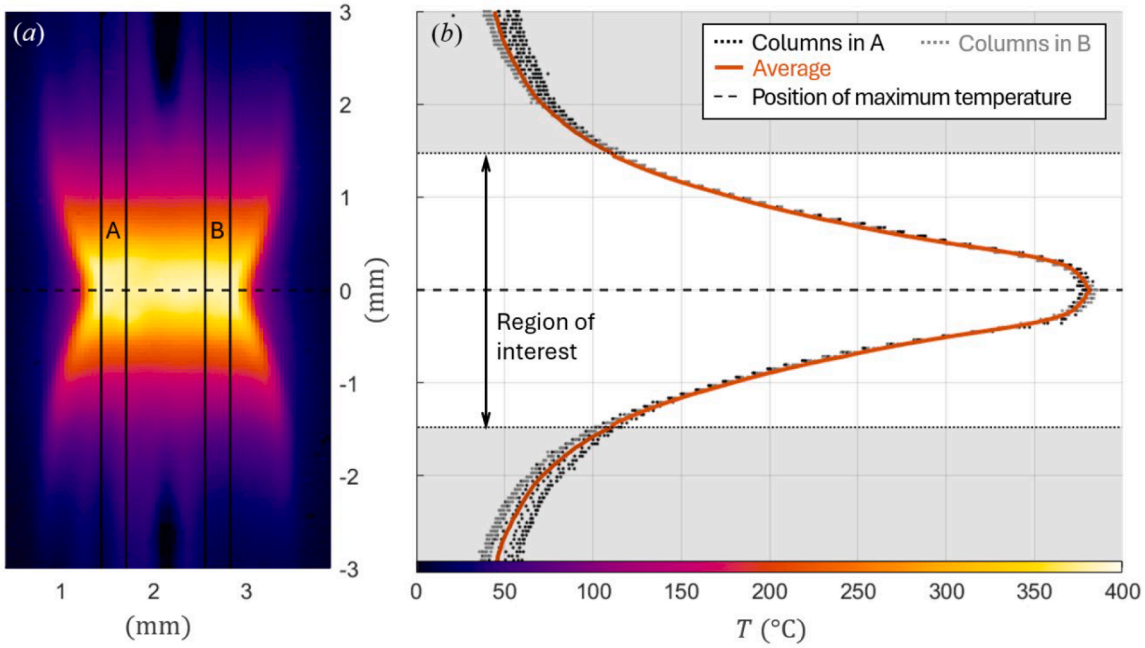

Fig. 10. Infrared images post-processing. (*a*) shows an infrared image (cropped for clarity) from a test at nominally 10/s highlighting the regions used for determining the axial distribution of superficial temperature. (*b*) plots the temperature distributions from region A, B along with the final averaged symmetrical profile.

tests. This is reasonable given the limited amount of uniform deformation observed. Therefore, temperature was assumed to remain constant at room temperature during the pre-necking phase.

Regarding post-necking characterization, for each test, all necking deformed configurations were considered, and the database approach was applied. As explained in Section 2, 3D loci of points representing the response of material points on the specimen's outer surface in the space $\varepsilon_{eq,pl} - \dot{\varepsilon}_{eq,pl} - \sigma_{eq}$ were identified.

It is important to note that Eqs. (3) and (5) remain applicable during necking. However, these equations provide estimates of strain and strain rate averaged over the cross-section, whereas the database values correspond to superficial strain and strain rate. Fig. 11 shows, for a test conducted at nominally 10/s, the time evolution, during necking, of both these evaluations at the minimum cross-section (i.e., strain and strain rate determined by analytical formulas versus those from the database). It is reasonable that, at the same instant, the analytical average values are higher than the superficial values from the database. This comparison emphasizes that, since the proposed method focuses on the sample's outer surface, using an analytical estimate of strain and strain rate is not advisable, as it may introduce to a non-negligible error.

Furthermore, the database approach allows for extracting information not only from the minimum cross-section, but also from a wider specimen's axial portion. While Eq. (5) for strain rate is easily applicable to the minimum cross-section, it is not immediately applicable to other cross-sections. This is because, to apply Eq. (5), the evolution of the radial coordinate of material points must be tracked, which would require knowing the axial displacement from one time to another. However, such axial displacement cannot be directly measured with the proposed experimental setup, which utilizes backlight illumination for better identification of the sample's external contour. Thus, the analytical estimate of strain rate is limited to the minimum cross-section, while the database approach allows for recovering the spatial distribution of strain rate along the specimen's outer surface.

Fig. 12 illustrates the material response determined by the proposed procedure. Being it a 3D locus of point, two planes $\dot{\varepsilon}_{eq,pl} - \varepsilon_{eq,pl}$ and $\sigma_{eq} - \varepsilon_{eq,pl}$ are used to present the results. To ensure that the loci of points were entirely within the plastic domain, a threshold strain rate was selected for each test and the parts of loci at lower strain rates were excluded.

The comparison of the results of different tests (only one test per condition is shown for sake of clarity) indicates the moderate positive strain rate sensitivity of the material. Examining the paths followed by the surface point at the profile center, it is immediately evident that the paths for the tests at nominally 1, 10, 10^3 s^{-1} are non-monotonic. This highlights that, despite the increasing strain rate experienced by that material point, the temperatures reached due to self-heating caused a considerable thermal softening of the material. Indeed, stainless steels tend to exhibit noticeable self-heating due to their low thermal conduction.

In the $\sigma_{eq} - \varepsilon_{eq,pl}$ planes, the true curves, computed using Eqs. (2) and (3), are also plotted. These curves represent the material behavior up the necking onset (thick dashed lines). However, during necking, these curves (thin dashed lines) significantly overestimate the stress because triaxiality is not accounted for in Eq. (2). Moreover, as highlighted in Fig. 3 in Section 2.1, during post-necking a strain rate sensitive behavior cannot be captured by a single curve in the $\sigma_{eq} - \varepsilon_{eq,pl}$ plane. Therefore, the database approach is used to estimate the loci of points that define the instantaneous states of the specimen's surface (gray solid lines of Fig. 12).

To analyze the strain rate effect within the single test, the lines in the plot $\sigma_{eq} - \varepsilon_{eq,pl}$ must be compared to each other. The degree of overlap among these lines qualitatively indicates strain rate dependence: the greater the divergence, the higher the strain rate sensitivity. This suggests that strain rate influences the results, especially for those at nominally 1, 10, 10^3 s^{-1}.

One could consider accounting for strain rate sensitivity, and implicitly considering the temperature effect, through a model like $\sigma_{eq} = f_I(\varepsilon_{eq,pl}, \dot{\varepsilon}_{eq,pl})$. This will be referred to as "Approach I". However, the main issue with this approach is that a different model is needed for each test and none of these models can be generalized to other applications. Implicitly incorporating the temperature means that the material model would only be valid in scenarios where the temperature experienced at a specific strain and strain rate matches that encountered (at that strain and strain rate) during the test used for calibration. This assumption is not generally valid.

Conversely, accounting for strain rate sensitivity while explicitly considering the temperature effect leads to a unique material model

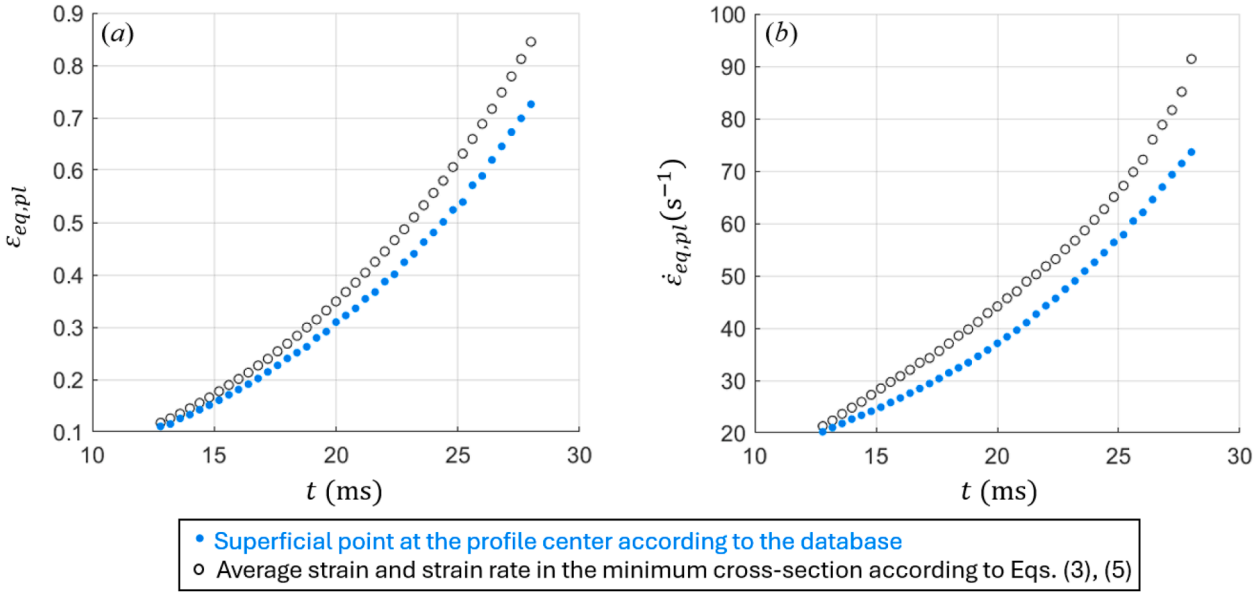

Fig. 11. Comparison between $\varepsilon_{eq,pl}$ and $\dot{\varepsilon}_{eq,pl}$ on the specimen surface and $\varepsilon_{eq,pl}$ and $\dot{\varepsilon}_{eq,pl}$ averaged over the minimum cross section.

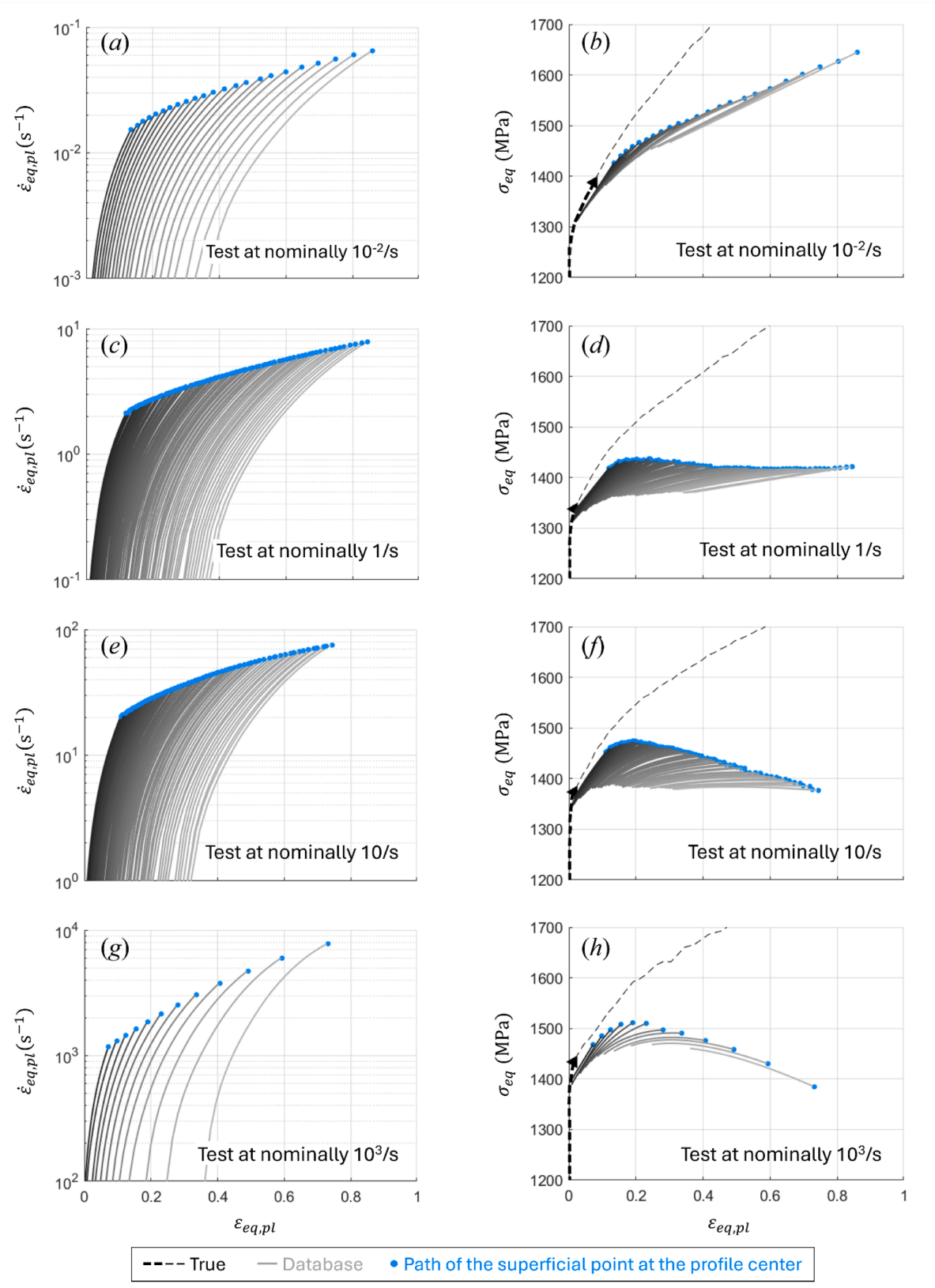

Fig. 12. Material response (in the space $\varepsilon_{eq,pl} - \dot{\varepsilon}_{eq,pl} - \sigma_{eq}$) during different tensile tests, according to the database predictions. One test for each type is shown for sake of clarity (the nominal strain rate is written on the plot).

$\sigma_{eq} = f_{II}(\varepsilon_{eq,pl}, \dot{\varepsilon}_{eq,pl}, T)$ able to represent the different tests (Approach II). This approach enhances reliability compared to Approach I, particularly in applications where the same strain and strain rate are reached at different temperatures relative to those reached during tests used for calibration. Although this requires extrapolating the model, the results would still be more reliable than those from Approach I. For this reason, the data obtained with the proposed approach was directly processed according to Approach II rather than Approach I.

However, it is fundamental to note that a model calibrated using dynamic tests performed at initial room temperature is applicable only to conditions where temperature increases are solely due to self-heating from initial room temperature. This is because temperature, generally, influences the material response either through the thermal activation of dislocation motion or by altering the material's structure (grain size, texture, etc.) [30]. In dynamic tests conducted at initial room temperature, only the thermal effects related to dislocation motion are involved. As a result, the identified model is restricted to scenarios where temperature influences only dislocation motion, not material structure.

To explicitly account for thermal softening, temperature data obtained from the infrared camera had to be incorporated. For each necking configuration, the database predictions of the distributions $\varepsilon_{eq,pl}(x)$, $\dot{\varepsilon}_{eq,pl}(x)$, $\sigma_{eq}(x)$ were combined with the temperature distribution $T(x)$ determined from the analyses of infrared images. This resulted in a point cloud in the 4D space $\varepsilon_{eq,pl} - \dot{\varepsilon}_{eq,pl} - \sigma_{eq} - T$, collecting information from all the different loading conditions.

Various strategies could then be adopted to develop a model from this data. From certain perspectives, the database approach is close to machine learning algorithms, as discussed in Beltramo et al. [22]. Therefore, while it is possible to fit the obtained data with a physical model, an empirical model aligns more closely with the overall procedure. Additionally, it was decided to avoid predefined dependencies on strain, strain rate and temperature. Instead of using existing empirical laws, a tabular definition was chosen, represented by the following equation:

$$\sigma_{eq} = f_1(\varepsilon_{eq,pl})\, f_2(\dot{\varepsilon}_{eq,pl})\, f_3(T). \tag{6}$$

This equation, like common empirical models, assumes an uncoupling between strain rate and temperature effects. This assumption is reasonable for the conditions analyzed in this paper, where temperature increases are limited to few hundred degrees due to self-heating, rather than varying initial temperatures. As mentioned earlier, the identified response (and temperature effect) can describe the material behavior under self-heating conditions.

Specifically referring to Eq. (6), $f_1(\varepsilon_{eq,pl})$ was derived from the quasi-static test, as previous analyses indicated that strain rate sensitivity at those strain rates could be neglected. For the coefficients $f_2(\log(\dot{\varepsilon}_{eq,pl}))$ and $f_3(T)$, after evaluating various functions, it was found that simple linear functions provided satisfactory results. Both f_2 and f_3 were set to 1 at room temperature and within the range of strain rates reached during the quasi-static test. Subsequently, $f_2(\dot{\varepsilon}_{eq,pl})$ and $f_3(T)$ were simultaneously optimized to fit the point cloud. The identified model fitted the point cloud with a deviation of 2%, computed as

$$\text{error} = \frac{1}{\sqrt{N}} \sum_{i=1}^{N} \frac{\sigma_{eq,i} - f_1(\varepsilon_{eq,pl,i})\, f_2(\dot{\varepsilon}_{eq,pl,i})\, f_3(T_i)}{\sigma_{eq,i}} \tag{7}$$

The functions f_2 and f_3 resulting from the optimization are reported in Fig. 13, alongside the cold curve $f_1(\varepsilon_{eq,pl})$.

The obtained model was implemented in Ansys LS-DYNA using *MAT_224 and structural-only FE simulations were run to evaluate the accuracy of the material model. The FE model was analogous to the one described in Section 2.2 except for the different geometry of the sample.

It is important to underline that structural-only simulations can be reliable only under isothermal or adiabatic conditions. Given the low thermal conductivity of 17-4PH, the tests at nominally 10 s^{-1} and 10^3 s^{-1} can reasonably be modeled as adiabatic. A Taylor–Quinney coefficient of 0.95 was used according to preliminary estimation, with the density and specific heat assumed to be 7800 kg/m^3 and 460 J/(kgK), respectively. Conversely, the test at 1 s^{-1} would require a coupled structure-thermal analysis, which will be explored in future works.

The results of FE simulations of tests are reported in Fig. 14, comparing them with experimental results in terms of radial engineering curves, geometric profiles and temperature profiles. It is interesting to notice that the shape of the geometric profile and that of the temperature distribution are quite similar. This similarity can be qualitatively understood considering that the stress does not vary significantly across the entire strain range, as illustrated in Fig. 12f and h:

$$T(x) = T_r + \frac{\beta}{\rho c_p} \int_0^{\varepsilon_{eq,pl}(x)} \sigma_{eq} d\varepsilon_{eq,pl} \approx T_r + \frac{\beta}{\rho c_p} \bar{\sigma}\, \varepsilon_{eq,pl}(x) \tag{8}$$

A good agreement with the experimental results is observed for all the tests, proving the potential of the method. Further improvements could be obtained by more deeply investigating the conversion of plastic work into heat.

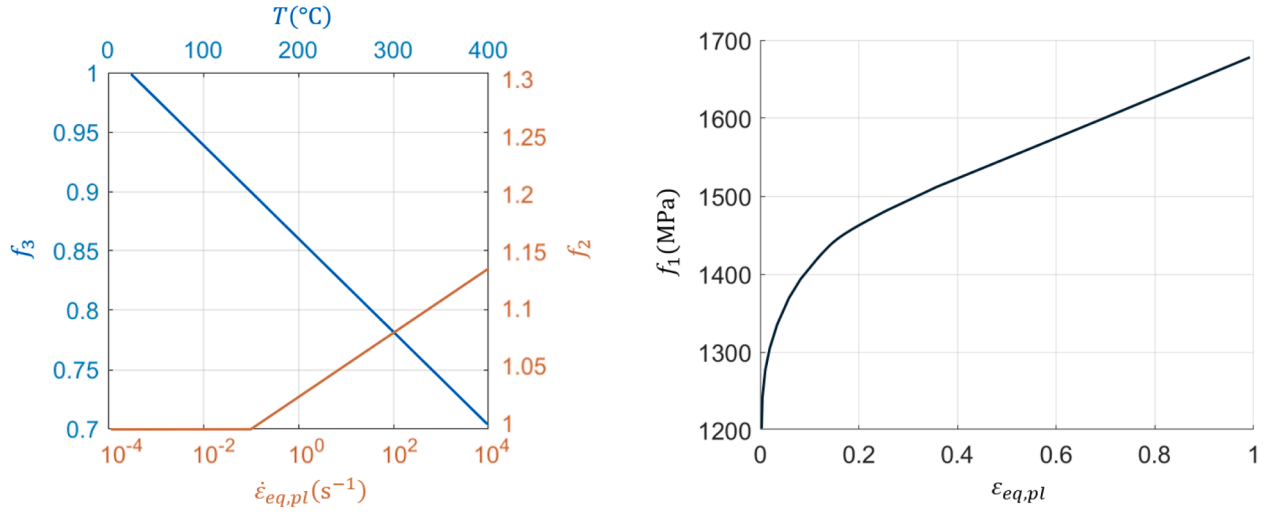

Fig. 13. Functions of the mathematical model $\sigma_{eq} = f_1(\varepsilon_{eq,pl})\, f_2(\dot{\varepsilon}_{eq,pl})\, f_3(T)$ representing the material behavior.

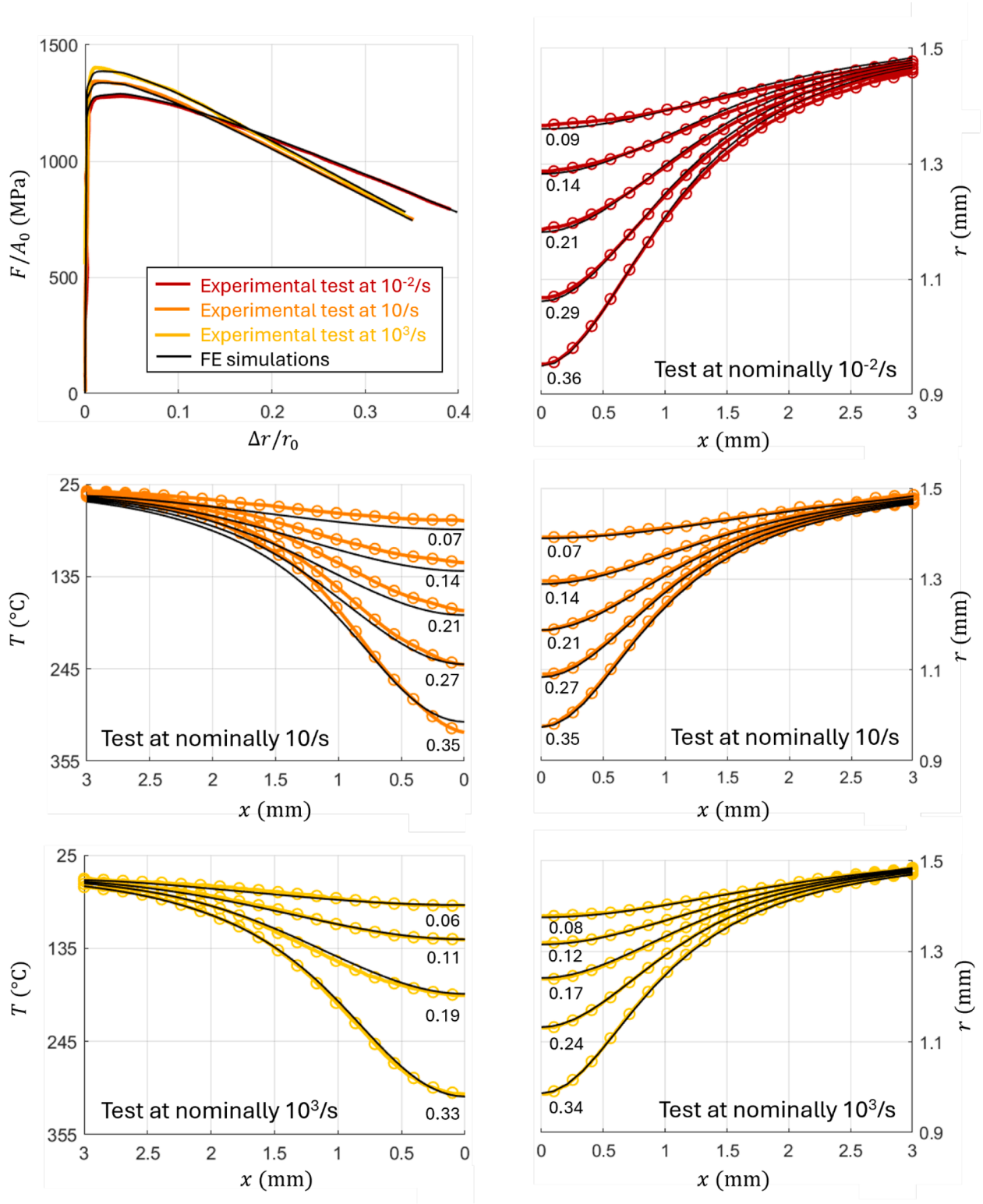

Fig. 14. Comparison between the experimental results and the FE results obtained using the identified plastic flow model. Only test types that could be considered under isothermal or adiabatic conditions were simulated and the comparison is presented in terms of engineering radial curve $F/A_0 - \Delta r/r_0$, necking profiles and temperature profiles (for dynamic tests). Next to each geometric and thermal profile, the corresponding value of $\Delta r/r_0$ is reported.

5. Conclusions

In the present work, the authors successfully adapted a method previously used for analyzing the post-necking phase of quasi static tensile tests for high strain rate tests. The proposed strategy is based on the principle that the necking shape of an axisymmetric specimen intrinsically contains information about the superficial distributions of strain, strain rate, and stress. Specifically, the method utilizes a database generated from numerical simulations to link the necking profile and engineering stress with the relationship between equivalent stress and

equivalent plastic strain.

Thus, the proposed approach requires minimal experimental effort for deformation analysis: it suffices to record the test with adequate spatial and time resolution and extract the specimen profile from acquired images, eliminating the need of DIC measurements. The computational cost is also reduced because a database is employed rather than a numerical optimization, and a strain rate insensitive database, appropriately reduced in size, has been shown to capture instantaneous response even of a strain rate sensitive material. Accuracy is ensured by relying on numerical results, which avoids introducing simplifying hypotheses about stress and strain fields and about material hardening behavior, aside from isotropic Von Mises material.

It is worth underlining that the output of the proposed method is a point cloud in the space $\varepsilon_{eq,pl} - \dot{\varepsilon}_{eq,pl} - \sigma_{eq}$, that in dynamic tests can be enriched with thermal information coming from the analysis of infrared images, resulting in a point cloud in the 4D space $\varepsilon_{eq,pl} - \dot{\varepsilon}_{eq,pl} - \sigma_{eq} - T$. This point cloud collects the quadruplets $(\varepsilon_{eq,pl}, \dot{\varepsilon}_{eq,pl}, \sigma_{eq}, T)$ experienced by superficial material points, instant by instant, during necking. As such, it reflects the material's visco-thermo-plastic behavior and can be subsequently fitted with the desired hardening law.

Therefore, the key outcome of the proposed method is the identification of the material response as a point cloud, without any a priori assumptions about the material behavior except for isotropic Von Mises plasticity. Only as a subsequent step can the point cloud be fitted with a specific hardening law.

The method's potential was demonstrated by applying it for characterizing a material over a wide range of strains and strain rates. An experimental campaign of tensile tests on martensitic stainless steel 17-4 PH proved the method's capability to address a strain rate sensitive material which also exhibits significant thermal softening in dynamic tests. Different loading conditions were simultaneously considered to identify a unique model representing the material response in case of self-heating. To be consistent with the proposed method itself, the authors opted for a tabular definition of the hardening law. In addition, multiplicative uncoupling of strain, strain rate and temperature effects was adopted. FE simulations using this material model accurately predicted experimental results of tests at nominally 10^{-2}, 10, 10^{3} s^{-1}. In dynamic tests, the model also provided satisfactory predictions for surface temperature profiles, despite the assumption of a constant Taylor–Quinney coefficient.

Future endeavors will focus on further exploiting temperature measurement to gain insights into non-adiabatic tests and to experimentally estimate the amount of plastic work converted into heat during tests under adiabatic conditions.

CRediT authorship contribution statement

Marta Beltramo: Writing – review & editing, Writing – original draft, Visualization, Validation, Software, Methodology, Investigation, Formal analysis, Data curation, Conceptualization. **Lorenzo Peroni:** Writing – review & editing, Validation, Supervision, Resources, Project administration, Methodology, Investigation, Conceptualization. **Martina Scapin:** Writing – review & editing, Validation, Supervision, Resources, Methodology, Investigation, Conceptualization.

Declaration of competing interest

The authors declare that they have no known competing financial interests or personal relationships that could have appeared to influence the work reported in this paper.

Data availability

The raw/processed data required to reproduce these findings cannot be shared at this time as the data also forms part of an ongoing study.

References

[1] Johnson GR. A constitutive model and data for metals subjected to large strains, high strain rates and high temperatures. In: *Proceedings of the 7th international symposium on ballistics, The Hague, Netherlands*, 1983; 1983.

[2] Zerilli FJ, Armstrong RW. Dislocation-mechanics-based constitutive relations for material dynamics calculations. J Appl Phys 1987;61(5):1816–25.

[3] Song B, Sanborn B. A modified Johnson–Cook model for dynamic response of metals with an explicit strain-and strain-rate-dependent adiabatic thermosoftening effect. J Dyn Behav Mater 2019;5(3):212–20.

[4] Gambirasio L, Rizzi E. On the calibration strategies of the Johnson–Cook strength model: discussion and applications to experimental data. Mater Sci Eng 2014;610:370–413.

[5] Zhang L, Gour G, Petrinic N, Pellegrino A. Rate dependent behaviour and dynamic strain localisation of three novel impact resilient titanium alloys: experiments and modelling. Mater Sci Eng 2020;771:138552.

[6] Kim JM, Park JS, Leem DH, Kim M, Barlat F, Pierron F, Kim JH. Determination of strain rate dependence at intermediate strain rates using acceleration information. Int J Impact Eng 2023;173:104482.

[7] Pierron F, Grédiac M. The virtual fields method: extracting constitutive mechanical parameters from full-field deformation measurements. Springer Science & Business Media; 2012.

[8] Marek A, Davis FM, Pierron F. Sensitivity-based virtual fields for the non-linear virtual fields method. Comput Mech 2017;60:409–31.

[9] Martins JMP, Thuillier S, Andrade-Campos A. Calibration of a modified Johnson–Cook model using the Virtual Fields Method and a heterogeneous thermo-mechanical tensile test. Int J Mech Sci 2021;202:106511.

[10] Park JS, Kim JM, Barlat F, Lim JH, Pierron F, Kim JH. Characterization of dynamic hardening behavior at intermediate strain rates using the virtual fields method. Mech Mater 2021;162:104101.

[11] Lee CS, Yoon JW, Woo SH, Park LJ. Thermal softening behavior up to fracture initiation during high-rate deformation. Int J Mech Sci 2023;251:108321.

[12] Sasso M, Newaz G, Amodio D. Material characterization at high strain rate by Hopkinson bar tests and finite element optimization. Mater Sci Eng 2008;487(1–2):289–300.

[13] Sedighi M, Khandaei M, Shokrollahi H. An approach in parametric identification of high strain rate constitutive model using Hopkinson pressure bar test results. Mater Sci Eng 2010;527(15):3521–8.

[14] Kajberg J, Wikman B. Viscoplastic parameter estimation by high strain-rate experiments and inverse modelling–Speckle measurements and high-speed photography. Int J Solids Struct 2007;44(1):145–64.

[15] Milani AS, Dabboussi W, Nemes JA, Abeyaratne RC. An improved multi-objective identification of Johnson–Cook material parameters. Int J Impact Eng 2009;36(2):294–302.

[16] Scapin M, Peroni L, Peroni M. Parameters identification in strain-rate and thermal sensitive visco-plastic material model for an alumina dispersion strengthened copper. Int J Impact Eng 2012;40:58–67.

[17] Zinovev A, Delannay L, Terentyev D. Plastic deformation of ITER specification tungsten: temperature and strain rate dependent constitutive law deduced by inverse finite element analysis. Int J Refract Metals Hard Mater 2021;96:105481.

[18] Majzoobi GH, Khosroshahi SFZ, Mohammadloo HB. Determination of materials parameters under dynamic loading: part II: optimization. Comput Mater Sci 2010;49(2):201–8.

[19] Scapin M, Peroni L, Carra F. Investigation and mechanical modelling of pure molybdenum at high strain-rate and temperature. J Dyn Behav Mater 2016;2:460–75.

[20] Yao D, Guan Y, Li M, Zhang Y, Duan Y. Inverse identification method for determining stress–strain curves of sheet metals at high temperatures. Eng Fract Mech 2023;284:109246.

[21] Beltramo M, Scapin M, Peroni L. An advanced post-necking analysis methodology for elasto-plastic material models identification. Mater Des 2023;230:111937.

[22] Beltramo M, Scapin M, Peroni L. An efficient shape-based procedure for strain hardening identification in the post-necking phase. Mech Mater 2024;196:105066.

[23] Scapin M, Beltramo M. A methodology for post-necking analysis in isotropic metals. Metals 2024;14(5):593.

[24] Chen S, Li WB, Wang XM, Yao WJ, Song JP, Jiang XC, Yan BY. Comparative study of the dynamic deformation of pure molybdenum at high strain rates and high temperatures. Materials 2021;14(17):4847.

[25] Tvergaard V, Needleman A. Analysis of the cup-cone fracture in a round tensile bar. Acta Metall 1984;32(1):157–69.

[26] Tu S, Ren X, He J, Zhang Z. Stress–strain curves of metallic materials and post-necking strain hardening characterization: a review. Fatigue Fract Eng Mater Struct 2020;43(1):3–19.

[27] Mirone G, Verleysen P, Barbagallo R. Tensile testing of metals: relationship between macroscopic engineering data and hardening variables at the semi-local scale. Int J Mech Sci 2019;150:154–67.

[28] Huh H, Ahn K, Lim JH, Kim HW, Park LJ. Evaluation of dynamic hardening models for BCC, FCC, and HCP metals at a wide range of strain rates. J Mater Process Technol 2014;214(7):1326–40.

[29] Song B, Chen W, Antoun BR, Frew DJ. Determination of early flow stress for ductile specimens at high strain rates by using a SHPB. Exp Mech 2007;47:671–9.

[30] Peroni L, Scapin M, Song B. Dynamic behavior of metals and alloys designed for high-temperature applications. Dynamic behavior of materials. Elsevier; 2024. p. 339–72.